Supporting Information

Unraveling the relationship between morphologies of metal-organic frameworks and properties of their derived carbon materials

Qiao Wu,[ab] Jun Liang,[a] Jun-Dong Yi,[a] Dong-Li Meng,[a] Peng-Chao Shi,[a] Yuan-Biao Huang*[ac] and Rong Cao*[ac]

[a]State Key Laboratory of Structural Chemistry, Fujian Institute of Research on the Structure of Matter, Chinese Academy of Sciences, Fuzhou 350002, China

[b]College of Chemistry and Materials Science, Fujian Normal University, Fuzhou 350007, China

[c]University of Chinese Academy of Sciences, Beijing 100049, China

Physical and chemical characterization

Powder X-ray diffraction (PXRD) patterns were recorded on a RigakuDmax 2500 diffractometer equipped with Cu-Kα radiation (λ= 1.54056 Å) over the 2θ range of 4-50° for MOFs and 4-80° for carbon materials with a scan speed of 3° min^{-1} at room temperature. Thermogravimetric analyses (TGA) were performed under a nitrogen atmosphere with a heating rate of 10 °C min^{-1} by using an SDT Q600 thermogravimetric analyser. N_2 sorption isotherms for MOFs and the derived carbon materials were measured by using a Micrometrics ASAP 2020 instrument at 77 K. Before the measurement, the samples were activated at 393 K in vacuum for 12 h. The transmission electron microscopy (TEM) and high resolution transmission electron microscopy (HRTEM) images were obtained on a FEIT 20 instrument at an accelerating voltage of 200 kV. Raman spectra of dried samples were obtained on Lab-RAM HR800 with excitation by an argon ion laser (532 nm). Elemental analyses of C, H, and N were carried out on an ElementarVario EL III analyzer. The morphologies of MOFs were studied using a (JSM-6700F) scanning electron microscope (SEM) working at 10 KV. X-ray photoelectron spectroscopy (XPS) measurements were performed on an ESCALAB 250Xi X-ray photoelectron spectrometer (Thermo Fisher) using an Al Kα source (15 kV, 10 mA).

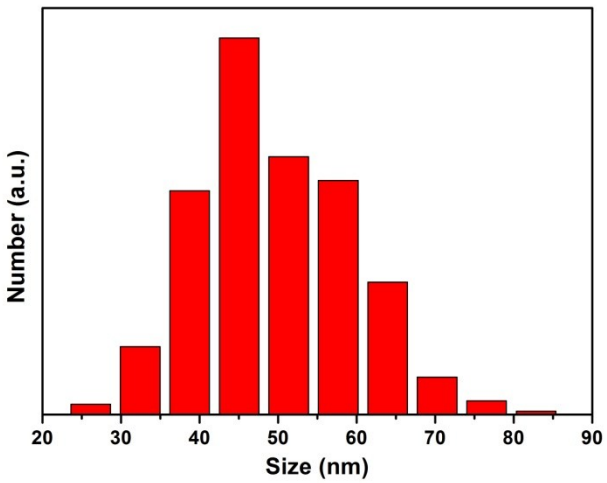

Fig. S1 Size distribution of 45 nm spherical shape ZIF-7-S (from a total number of 400).

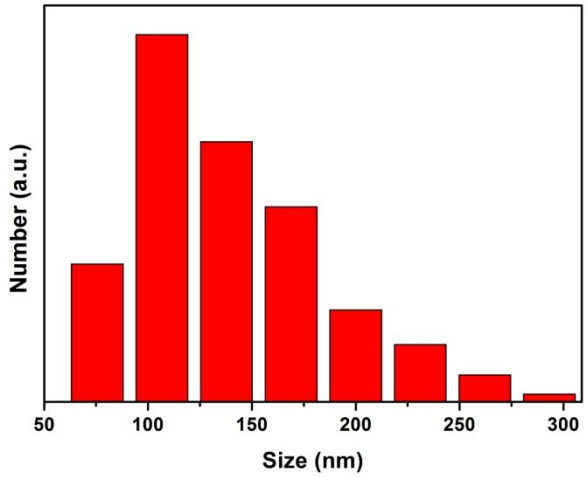

Fig. S2 Size distribution of 125 nm polyhedral shape ZIF-7-D (from a total number of 300).

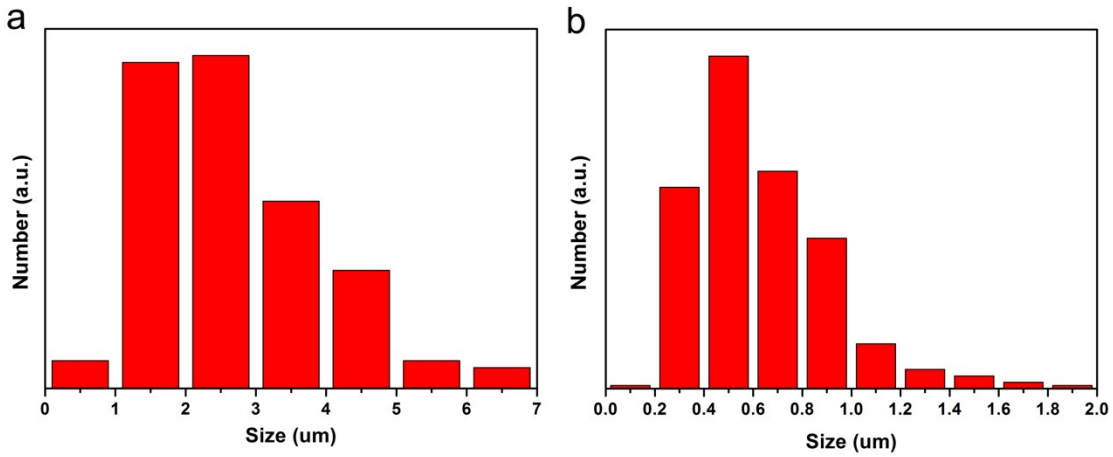

Fig. S3 Rod ZIF-7-R with (a) 3μm in length and (b) 0.6 μm in diameter.

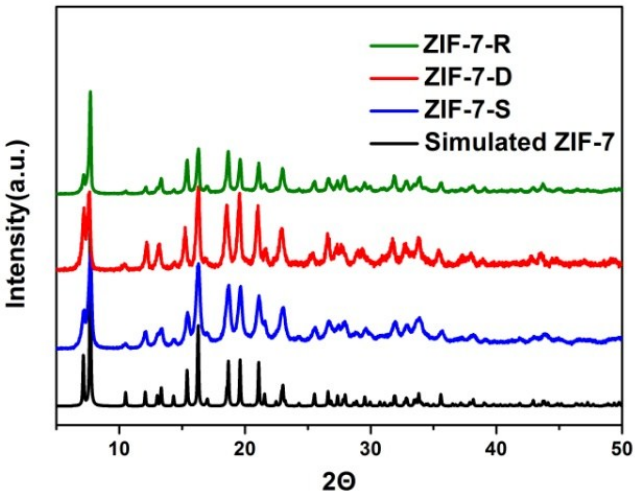

Fig. S4 PXRD patterns of ZIF-7-S, ZIF-7-D and ZIF-7-R.

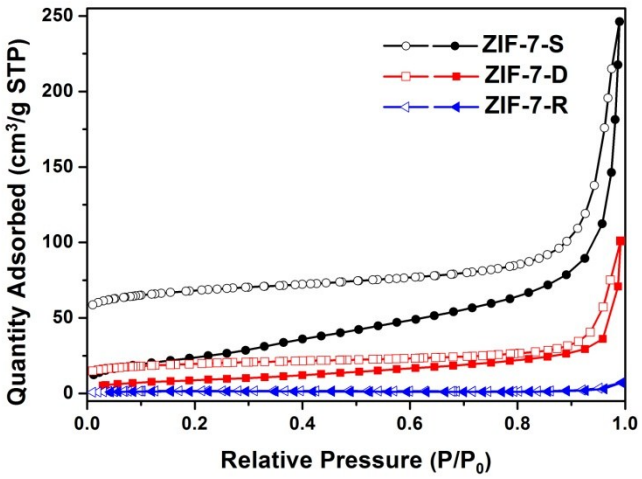

Fig. S5 N_2 sorption isotherms of ZIF-7-S, ZIF-7-D and ZIF-7-R.

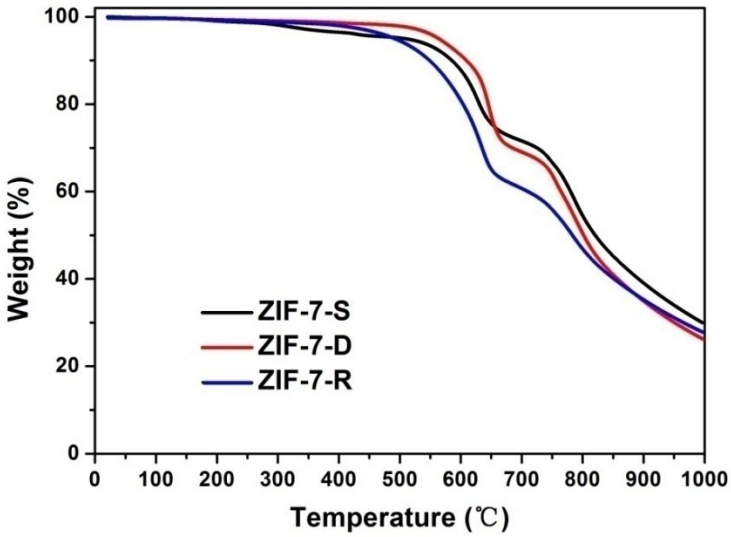

Fig. S6 Thermogravimetric analysis (TGA) of ZIF-7-S, ZIF-7-D and ZIF-7-R.

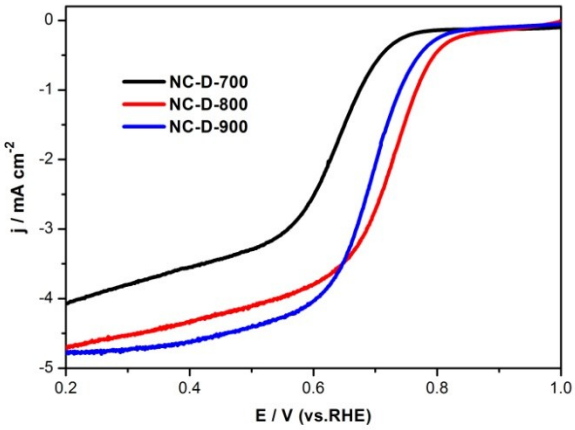

Fig. S7 Liner sweep voltammetry (LSV) curves for NC-D-700, NC-D-800 and NC-D-900 at an RDE rotation rate of 1600 rpm with a scan rate of 5 mVs^{-1}.

We have investigated the effect of different carbonization temperatures for NC-D-*x* (*x* = 700, 800, 900) materials on the performance of ORR reactions. The LSV measurement results of the NC-D-*x* prepared at different temperatures were shown in Fig. S7. NC-D-800 showed the most positive onset (0.87 V *vs* RHE), which was superior to NC-D-700 (0.77 V) and NC-D-900 (0.83 V), suggesting a pronounced electrocatalytic activity of NC-D-800 for ORR.

Table S1 Textural properties of ZIF-derived porous N-doped carbon materials.

Sample	BET surface area ($m^2 g^{-1}$)	Total pore volume ($cm^3 g^{-1}$)
NC-S-800	352	0.43
NC-D-800	538	0.41
NC-R-800	272	0.17
NC-D-NH_3	636	0.54

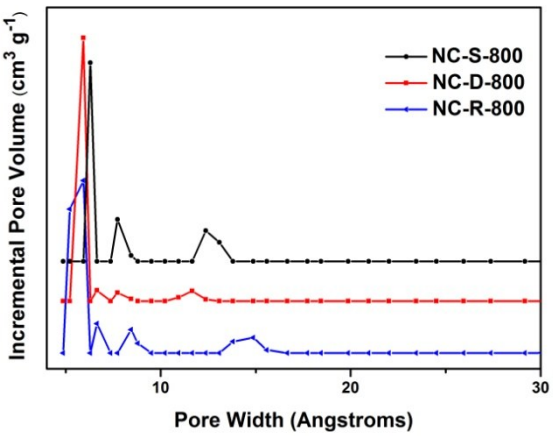

Fig. S8 Pore size distributions of NC-S-800, NC-D-800 and NC-R-800, respectively.

Table S2 Nitrogen atom percentage of obtained porous N-doped carbon materials.

Sample	Ncontent (wt%)[a]	Ncontent (wt%)[b]	pyridinic-N (%)	pyrrolic-N (%)	graphitic-N (%)	pyridine-N-oxide (%)
NC-S-800	11.05	9.91	37.7	30.9	25.3	6.1
NC-D-800	10.30	9.42	39.5	23.3	30.4	6.8
NC-R-800	10.24	8.58	38.3	25.7	28.4	7.6
NC-D-NH_3	2.28	2.09	19.1	13.2	54.6	13.1

[a]Based on elemental analysis results.

[b]Based on X-ray photoelectron spectroscopy (XPS).

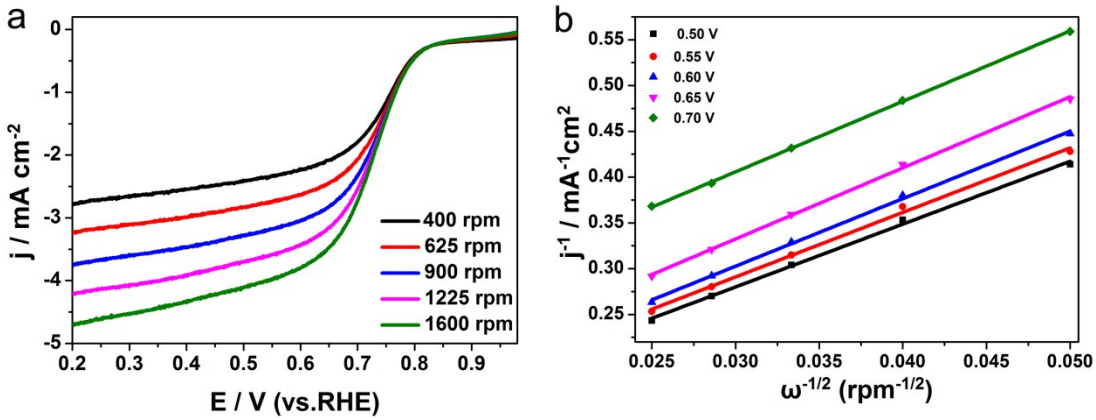

Fig. S9 (a) LSV curve of NC-D-800 at different rotation rates, (b) Linear fitting curve of K-L plots.

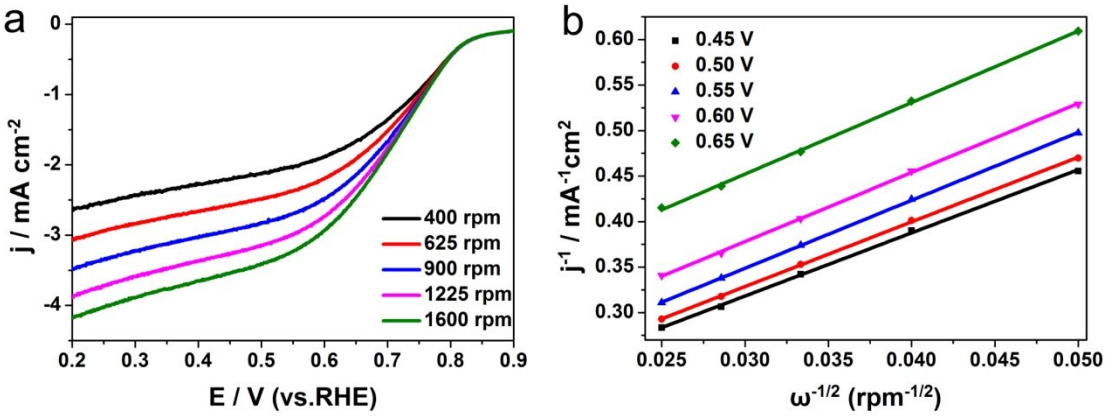

Fig. S10 (a) LSV curve of NC-S-800 at different rotation rates, (b) Linear fitting curve of K-L plots.

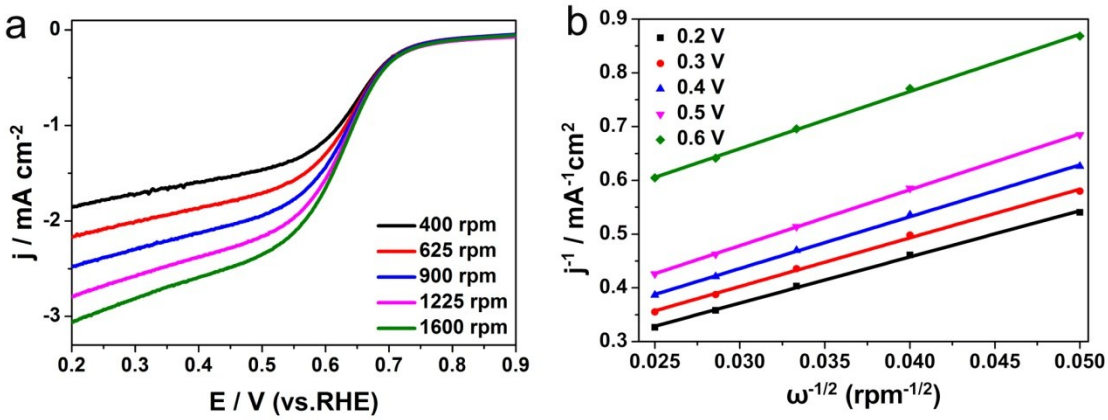

Fig. S11 (a) LSV curve of NC-R-800 at different rotation rates, (b) Linear fitting curve of K-L plots.

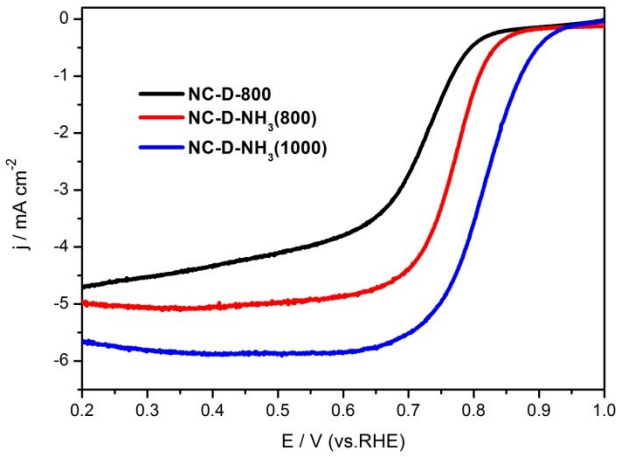

Fig. S12 Liner sweep voltammetry (LSV) curves for NC-D-800, NC-D-NH_3(800) and NC-D-NH_3(1000) at an RDE rotation rate of 1600 rpm with a scan rate of 5 mVs^{-1}.

NC-D-800 was treated at 800 ^{o}C for 30 min under flowing NH_3 to obtain NC-D-NH_3(800), while treated at 1000 ^{o}C for 30 min under flowing NH_3 to obtain NC-D-NH_3(1000).

The LSV measurement results of the NC-D-NH_3(x) (x = 800, 1000) prepared at different temperatures were shown in Fig. S12. NC-D-NH_3(1000) showed the best ORR activity with the most positive onset of 1.0 V (*vs* RHE) and half-wave potentials of 0.82 V, which was superior to NC-D-NH_3(800) with positive onset of 0.89 V and half-wave potentials of 0.77 V. Furthermore, compared with the NC-D-NH_3(800), NC-D-NH_3(1000) showed higher diffusion-limiting current density of 5.65 mA cm^{-2} at 0.2 V, indicating that NC-D-NH_3(1000) obtained at 1000 degrees with NH_3 atmosphere has better ORR activity.

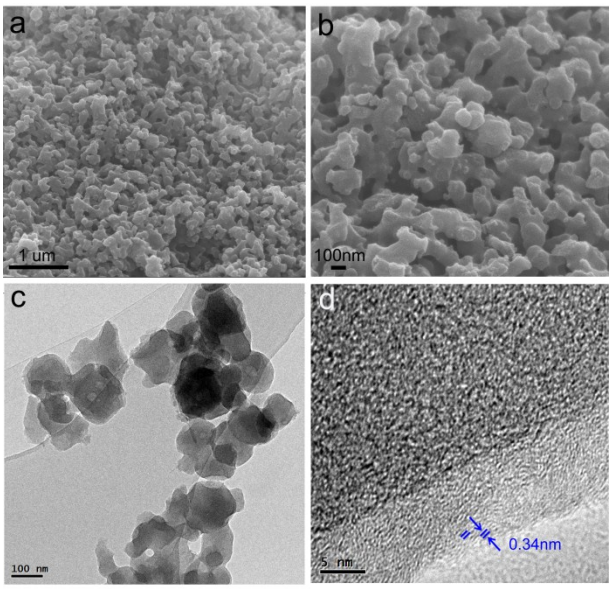

Fig. S13 The NC-D-NH_3 of (a-b) SEM images with different scale bars, (c) TEM image (d) HRTEM image.

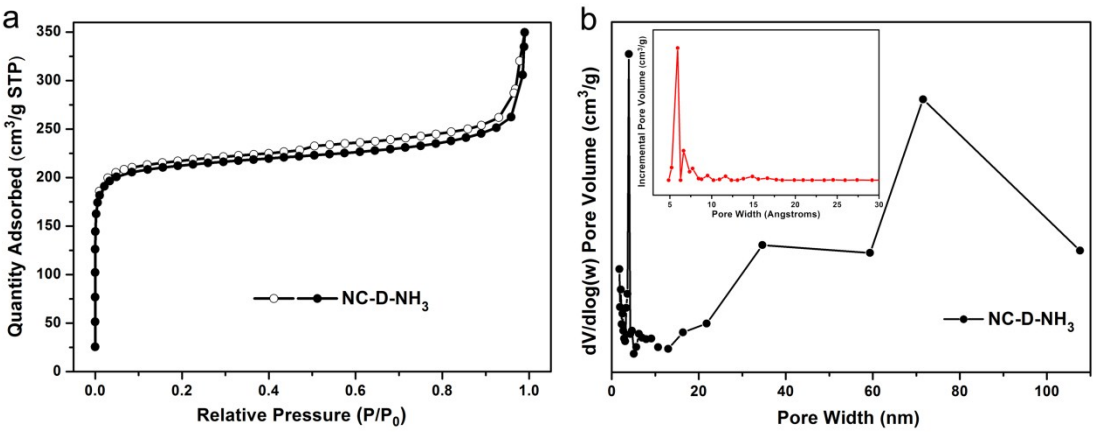

Fig. S14 (a) N_2 sorption isotherms and (b) pore size distributions for NC-D-NH_3. Solid symbols denote adsorption, open symbols denote desorption (P/P_0 = partial pressure).

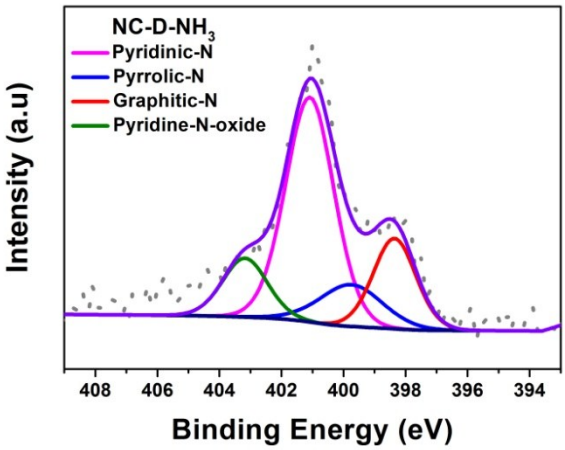

Fig. S15 N 1s spectra of NC-D-NH_3 with four kinds of nitrogen species (pyridinic-N, pyrrolic-N, graphitic-N, and pyridinic-N-oxide)